The 9th European Congress on Computational Methods in Applied Sciences and Engineering
ECCOMAS Congress 2024
3 – 7 June 2024, Lisboa, Portugal

NUMERICAL SIMULATION OF VECTORING OF ARC PLASMA JET USING COANDA EFFECT

M. MODANLOUJOUBARI[*], F. DOLATI[*], M. ABDOLLAHZADEH[†], H. DEYLAMI[*], J. C. PÁSCOA[†] AND F. RODRIGUES[†]

[*] Faculty of Mechanical Engineering
University of Guilan, Rasht, Iran
e-mail: siyavash.mojo@gmail.com, farid.dolati@gmail.com, hmohaddesd@gmail.com

[†] C-MAST- Center for Mechanical and Aerospace Science and Technology
Universidade da Beira Interior, Covilhã, Portugal
email: mm.abdollahzadeh@ubi.pt, pascoa@ubi.pt, fmfr@ubi.pt

Key words: Coanda effect, Plasma spray, Numerical simulation, Control flow, jet deflection.

Summary. The fluidic thrust vectoring method uses a curved surface and secondary flow to enhance the Coanda effect near the surface. This approach does not require mechanical parts, resulting in a lighter, simpler system with reduced maintenance and repair costs. In the present study, the outflow of a plasma torch controlled by the fluidic thrust vectoring method has been investigated. Numerical simulations were conducted over a 6-second flow period for operating conditions of 50 SLPM flow rate and 500 A electrical current. The fluidic thrust vectoring method was examined for three Coanda surfaces radius, three secondary flow heights, and three gaps between the secondary and primary jets. A 3D numerical simulation of the plasma torch was performed, obtaining velocity, temperature, and other properties at the torch outlet, which were then used as inputs for the final geometry. A two-dimensional solution was carried out to investigate the effects of the Coanda surface and secondary flow on the deflection of the plasma jet. The results demonstrate that increasing the mass flow ratio without considering the geometry leads to an increase in the thrust vector angle, which is also dependent on geometry. Changes in the dimensions can cause either a decrease or increase in the dead zone, thereby delaying the positive jet deflection angle.

1 INTRODUCTION

Thrust vectoring (TV) is a method commonly used in aerospace vehicles to alter and control the direction of thrust trajectory [1,2]. Thrust vectoring techniques comprise the fluidic thrust vectoring (FTV) and mechanical thrust vectoring (MTV) which are two distinct approaches for controlling the attitude and trajectory of aerospace vehicles. Mechanical thrust vectoring involves mechanical components to deflect the direction of the flow of the exhaust gases. The fluid-based thrust vectoring is a more recent method and has advantages over the mechanical-based thrust vectoring such as simplicity and lower weight [3]. FTV employs secondary jets to manipulate the primary exhaust flow and uses the injection of a tangential flow (co-flow thrust) to control the main jet direction. This allows to perform the flow trajectory control without

using mechanical components which reduced the weight and momentum losses of the system [4]. For achieve this, co-flow thrust vectoring control uses the Coanda effect at the nozzle exit to efficiently deflect and vectorize the outlet jet. When a fluid flow moves near a curved surface, the kinetic movement of the flow creates a pressure gradient near the wall which, in turn, leads the fluid to attach to the surface naturally. This phenomenon was firstly revealed by Henri Coanda and, due to that, is commonly designated as Coanda effect [4,5]. For improving the knowledge about the Coanda effect, Newman [6] conducted basic experimental investigations on jets deflection around a circular cylinder. His study indicated that the Coanda phenomenon is a direct consequence of the balance of centrifugal force and radial pressure produced by the interaction of the fluid and the curved wall surface [7,8]. Several experimental and computational investigations were conducted in order to study the Coanda effect generated in flows around cylinders or curved walls with different radius, at different Reynolds numbers and different slot widths [9–12]. These works demonstrated that to change the angle of deviation (or separation), the momentum of the main flow should be reduced or the radius of the Coanda surface should be changed. Juvet proposed a configuration for controlling high Reynolds number round jets with a secondary flow between the main jet and the Coanda surface. He carried out tests for various momentum ratios with constant slot width and Coanda surface radius. They concluded that for momentum ratios between 0- 0.1 Coanda surfaces have a low effect on the primary jet but by increasing the momentum ratios above 0.1 the primary jet could be effectively vectored [13]. Mason & Crowther [14] explained that there are three important zones of control response in fluidic thrust vectoring. At low momentum flow ratios, the jet is vectored in reverse direction and these zones are called the dead zones. By increasing the momentum flow ratio, the vectoring angle is increased and can be controlled in the desirable direction. This second zone of operation is designated as active zone. The third and last zone is called the saturation zone, since in this zone the vector angles will no longer increase with the increase of the momentum ratio. Banazadeh et al. [15] studied the deflection of the exhaust jet on a small gas turbine by implementing the co-flow method. The maximum deflection angle obtained was 23 degrees for a 57 mm Coanda surface radius and 1.4 mm secondary flow slot height. In addition, they concluded that by increasing the secondary flow rates, the jet deflection angle increases as well. Al-Asady and Abdullah [16] carried out an experimental and numerical investigation on various mass flow ratios, secondary flow heights, and Coanda surface diameters for a 3D rectangular duct. The results showed that increasing the secondary mass flow ratio led to an increase in the jet deflection angle, but the secondary gap height showed an inverse relation with the jet deflection angle. Both the experimental and computational results corroborated this trend. Mason and Crowther [17] also performed experiments using co-flow TVC method but, in their study, they focused on swept and non-swept nozzles at different low Mach numbers. They verified that the swept nozzle presented a more linear influence over a range of blowing ratios, while the non-swept nozzle showed a non-linear control region. They concluded that swept nozzles have better effectiveness and efficiency than non-swept nozzles. Ahmad et al. [18] presented numerical and experimental results related to a co-flow method fluidic thrust vectoring concept. They studied different ratios of Coanda surface radius (R) and secondary slot height (h), at constant primary flow height, for different mass ratios of secondary to primary jets. The results indicated that as the ratio R/h increases, the angle of primary jet deflection becomes steeper, and the response speed of the vectored jet gets quicker. The experimental results were compared with the predictions of numerical analyses and

demonstrated a good agreement. Fig. 1 shows a schematic of the co-flow fluidic thrust vectoring system and identifies the main geometrical parameters that, according with the literature stated above, have higher influence in the effectiveness of the outlet jet vectorization. As represented in Figure 1, the main geometrical parameters are the Coanda surface ratio (R), the secondary flow height (h), the primary flow hydraulic diameter (D) and the gap between the primary and secondary flow (g).

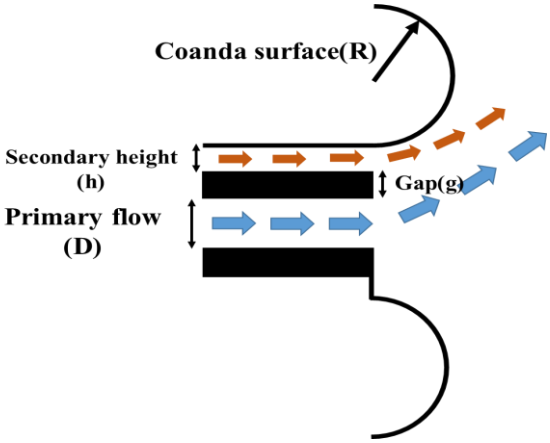

Figure 1: Schematic of the co-flow FTV system.

During the recent years plasma technologies have gained an increased interest for different types of applications [19–22]. Plasma technologies are commonly divided in two distinct groups: thermal plasmas and non-thermal plasmas [23–25]. Thermal plasmas are nearly fully ionized, achieve temperatures extremely larger than non-thermal plasmas and the electrons, ions, and neutral particles are in thermal equilibrium. On the other hand, non-thermal plasmas are only partly ionized and present a significant temperature difference between the electrons and the heavy particles [26–28]. Non-transferred arc plasma torches (thermal plasma) are technologies that use plasma as a heat source for plasma spray coating, chemical and powder synthesis, and toxic waste treatment [29]. In these technologies, plasma jets are used as directed sources since they present very high energy and momentum. A conventional plasma torch consists of a nozzle that acts as an anode and a cathode that is located coaxially with of the anode. Plasma torches can also be used in space applications, where light, small, and efficient propellants are needed [30]. In this case, DC or AC arc discharge in the nozzle exiting area can be used for obtaining momentum and induce a flow velocity usually higher than with chemical thrusters. Thermal energy is converted into kinetic energy when expanding through a nozzle like other conventional systems. Although this working principle is very similar to chemical thrusters, higher velocities can be achieved due to the independence of the content of the propellant energy source. Plasma jet can produce almost twice as much thrust as chemical thrusters and by that they allow to reduce weight, which is very important in space applications [31]. However, the control of the plasma jet direction is very challenging since, due to high temperature of thermal plasma, if the jet hits the nozzle walls, it will lead to fast degradation and erosion of the it.

Considering the potential of fluidic thrust vectoring control methods to manipulate flows,

the purpose of this research is to implement the control method to deflect the plasma jet using a secondary flow. By using a secondary co-flow along with outlet Coanda surfaces, the plasma jet can be vectorized and controlled and, in simultaneous, the secondary flow avoids the direct contact between the plasma and the nozzle walls, increasing the durability and reliability of the device. Initially, tridimensional and transient simulations of the plasma torch Will be performed. These initial simulations will allow to obtain the properties as velocity and temperature which will used as boundary conditions for the simulations of the co-flow control over the plasma jet. Thus, in the second part of the study, the outlet flow control of a plasma torch under the influence of the Coanda effect will be investigated. The influence of geometrical and flow variables will be studied, which include the radius of the Coanda surface, the height of the secondary flow, the gap between the secondary and the main flow and the mass flow rate ratio between the two flows.

2 MODEL DESCRIPTION

The main purpose of this study is to investigate the outlet flow of a plasma torch under the influence of the Coanda effect. In this study, the geometry includes a main flow that exits from the plasma torch, the Coanda plane is concentric with the torch and the secondary flow enters from the upper side of the main flow. The diameter of the plasma torch outlet (D) is 8 mm while the height of the secondary flow (h), the distance between the main and secondary flow (g), and the collar radius (R) will be variable (Fig. 1). This system is designed to control the direction of the jet without using mechanical moving parts and by using a secondary flow control along with Coanda effect.

2.1 Model Assumptions for plasma

For the simulations the continuum assumption and the quasi-neutrality condition are considered, meaning that the plasma is assumed as a compressible perfect gas in local thermodynamic equilibrium (LTE). Gravitational effects and viscous dissipation are considered negligible, and the plasma is optically thin. In the plasma arc region, the induced electric field is negligible in comparison with the applied electric field intensity. Because of the lower electric conductivity near the cold boundary of the electrode, the vicinity of the anode (within a distance of 0.1 mm) is artificially considered as a medium with high electrical conductivity of 10^4 S/m.

2.2 Governing Equations

Based on the foregoing assumptions, the governing equations for the 3D time-dependent model for the arc plasma can be written as follows:

Conservation of mass:

$$\frac{\partial \rho}{\partial t} + \nabla \cdot \left(\rho \vec{V}\right) = 0 \tag{1}$$

Conservation of momentum:

$$\rho\left(\frac{\partial \vec{V}}{\partial t} + \vec{V} \cdot \nabla \vec{V}\right) = -\overrightarrow{\nabla P} + \mu_{eff} \nabla^2 \cdot \vec{V} + \vec{j} \times \vec{B} \tag{2}$$

Conservation of energy:

$$\rho c_p \left(\frac{\partial T}{\partial t} + \vec{V} \cdot \nabla T\right) = \nabla \cdot \left(\kappa_{eff} \nabla T\right) + \frac{DP}{Dt} + \vec{j} \cdot \vec{E} - S_r \tag{3}$$

Maxwell electromagnetism equations:

$$\nabla \cdot (\sigma \nabla \phi) = 0 \tag{4}$$

$$\vec{E} = -\nabla \phi \tag{5}$$

$$\nabla^2 \vec{A} = -\mu_o \vec{j} \tag{6}$$

$$\vec{B} = \nabla \times \vec{A} \tag{7}$$

Ohm's law:

$$\vec{j} = \sigma \vec{E} \tag{8}$$

where ρ is gas mass density, t the time, $\vec{V}$ the velocity, $\vec{j}$ the electric current density, $\vec{B}$ the magnetic induction vector, P the gas pressure, μ the dynamic viscosity, C_p the specific heat at constant pressure, $\vec{E}$ the electric field, S_r the volumetric net radiation losses, k the gas thermal conductivity, σ the electric conductivity, ϕ the electric potential, $\vec{A}$ the magnetic vector potential and μ_0 the permeability of free space. The thermodynamic and transport properties of the plasma gas are taken from Murphy & Arundelli [32] and Colombo et al. [33] .

2.3 Computational Domain and Boundary Conditions

The geometry used in the current work for simulating the plasma torch is based on Huang et al. [34] shown in Fig. 2. The computational domain formed by the region inside the torch is limited by the cathode, the gas flow inlet, the anode, and the outlet as shown in Fig.2.

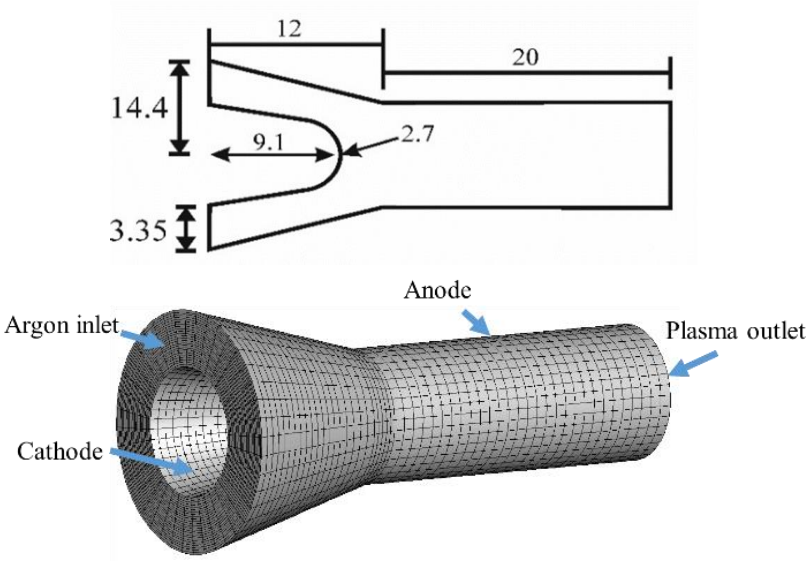

Figure 2: Computational domain, mesh and boundary sides.

The computational domain is meshed using 252,480 hexahedral cells. In this study, for gas flow calculations, the Standard k-ε model is employed. The governing equations are solved by FLUENT with the SIMPLE algorithm. As seen in Fig. 2, the boundary of the computational domain is divided into 4 different faces to allow the specification of boundary conditions. Table 1 shows the boundary conditions used in the simulation.

Table 1: Boundary conditions

Boundary	**P(Pa)**	**V**	**T**	**ϕ**	**A**
Inlet	111325	50 SLPM	300 k	$\frac{\partial \phi}{\partial \eta} = 0$	$\frac{\partial A}{\partial \eta} = 0$
Cathode	$\frac{\partial P}{\partial \eta} = 0$	0	T(r)	j(r)	$\frac{\partial A}{\partial \eta} = 0$
Anode	$\frac{\partial P}{\partial \eta} = 0$	0	q_a	0	$\frac{\partial A}{\partial \eta} = 0$
Outlet	101325	$\frac{\partial V}{\partial \eta} = 0$	$\frac{\partial T}{\partial \eta} = 0$	$\frac{\partial \phi}{\partial \eta} = 0$	$A = 0$

Where:

$$T(r) = 300 + 3000 \exp\left(-\left(\frac{r}{R_c}\right)^{n_c}\right) \tag{9}$$

$$j(r) = j_{cath_0} exp\left(-\left(\frac{r}{R_c}\right)^{n_c}\right) \tag{10}$$

After simulating the plasma torch, a second part of the work was performed for understanding the ability of using fluidic thrust vectoring method to control the plasma jet. The computational grid used for this second part of the study is presented in Figure 3. As can be seen, for ensuring the accuracy of the results without excessively increase the computational cost, the mesh was refined in the regions where larger gradients are expected.

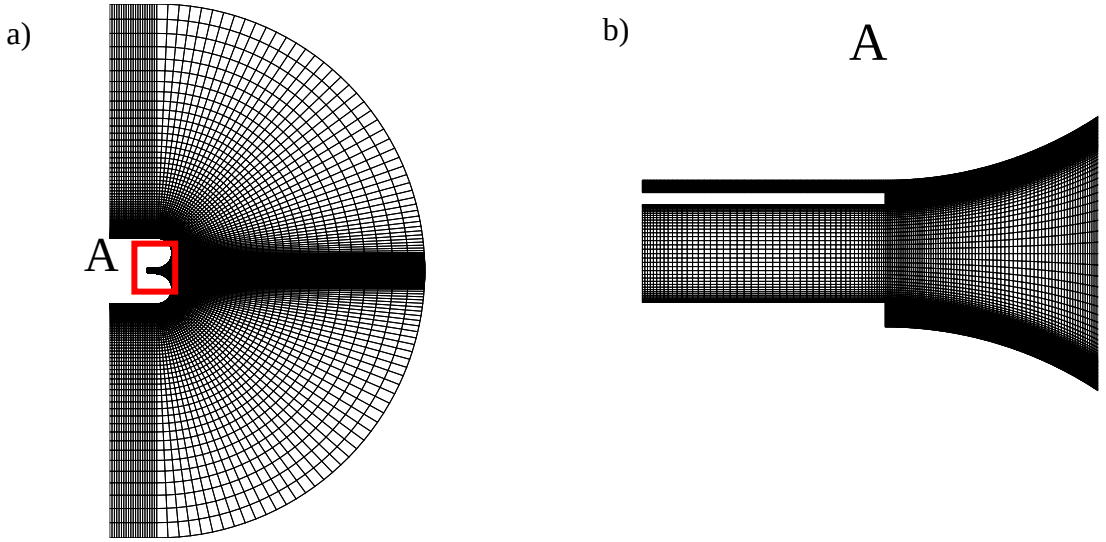

Figure 3: Computational grid (a) Full computational grid (b) mesh around the nozzle outlet and Coanda surface.

In this study, the influence of geometrical and flow variables on the outlet flow of a plasma torch was investigated. The geometrical variables include the radius of the Coanda surface, the height of the secondary flow, and the gap between the secondary and the main flow. The variation of the mass flow rate of the secondary flow was also considered for the analysis. To compare the results, the deviation angle has been computed as described in the following equation:

$$\theta = tan^{-1}\left(\frac{F_y}{F_x}\right) = \tan^{-1}\left(\frac{\sum \dot{m}V_y}{\sum \dot{m}V_x}\right) \tag{11}$$

To determine the effect of the key parameters on plasma jet vectorization, numerical simulations were carried out. The study considered the application of about 6 different mass flow ratios between 0.0625-0.116, various Coanda surface radius ratios (1, 2 and 4), different secondary flow height ratio (0.125, 0.1875 and 0.25) and various gaps between the secondary and primary jet ratio (0.0625, 0.125 and 0.1875).

3 SIMULATION RESULTS AND DISCUSSION

3.1 Flow Fields Inside the Torch

The current density distribution inside the plasma torch calculated by the LTE model is shown in Fig. 4(a). Fig. 4(b) shows electric potential distribution inside the plasma torch at 420μs. The gas temperature and velocity distributions inside the plasma torch are shown in Fig. 5.

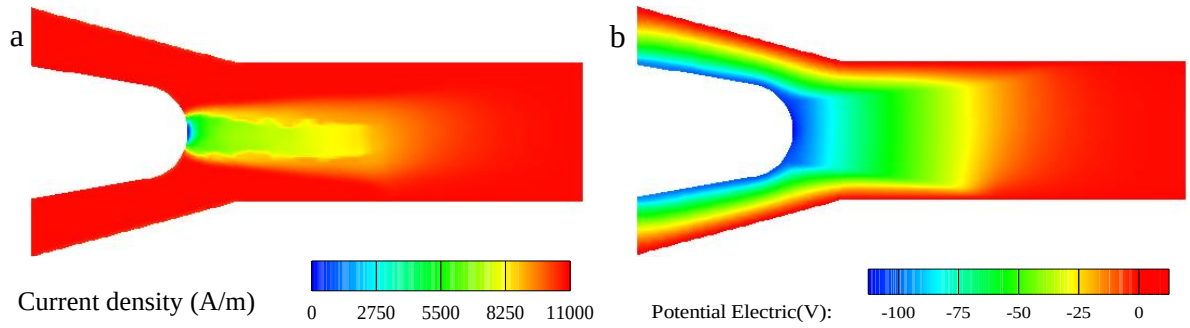

Figure 4: Distribution of a) electric current density and b) electric potential inside the plasma torch at t= 420μs.

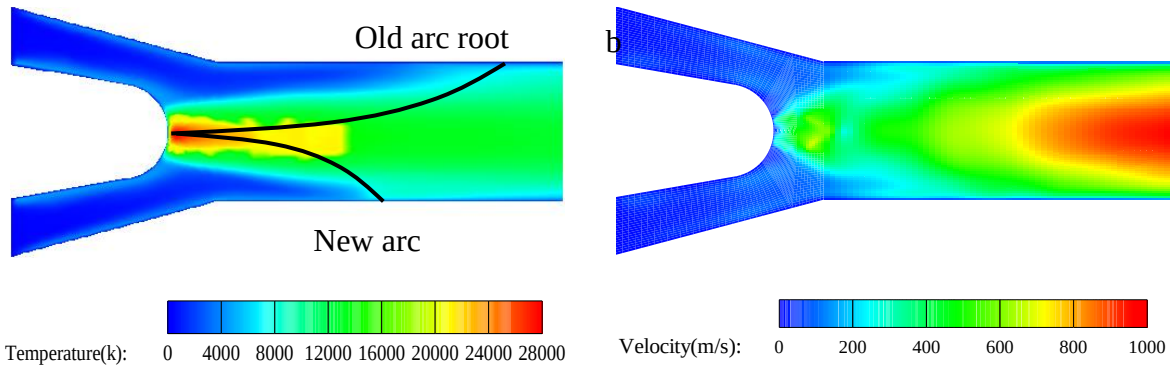

Figure 5: Distribution of a) temperature and b) velocity inside the plasma torch at t= 420μs.

As can be seen, the two arc roots are formed and after that, the electric current goes through the old arc root and the new one simultaneously. As time elapses, the old arc root disappears and only the new one will remain. It indicates that the temperature distributions of arc bend and deviate to the contrary side because the electrical current passes mainly through the arc root. The fluctuations of plasma gas temperature and velocity are the main causes of plasma jet fluctuation. For the plasma jet conditions of argon gas, 500 A electric current and 50 SLPM gas flow rate, the maximum gas temperature achieves more than 14000K and the velocity reaches more than 1000 m/s. The values obtained for T_{ave} and V_{ave} are 9500K and 700 m/s, respectively. The results herein obtained will now be used as boundary conditions for the simulations of applying the fluidic thrust vectoring method to control the direction of the outlet plasma jet.

3.2 Plasma Jet deflection using Co-flow FTV method

3.2.1 Influence of the Coanda surface radius

Two-dimensional numerical simulations of plasma jet control by co-flow nozzle are conducted to predict the jet deflection. When the secondary flow is not applied, the main flow enters the environment without any change or deviation. With activation of the secondary flow, according to the mass flow ratio applied, the deviation of the main flow can be controlled. The secondary flow also disturbs the force balance of the flow. On the side that the secondary flow is applied, less pressure is generated near the wall compared to on the other side of the jet. Due to that, the jet begins to deflect towards the Coanda surface. Figure 6 shows the jet deflection angle at different mass flow ratios and different Coanda surface radius. In addition, the velocity distribution related to the mass flow ratio of 0.116 for three Coanda surface radius is shown in Fig. 7.

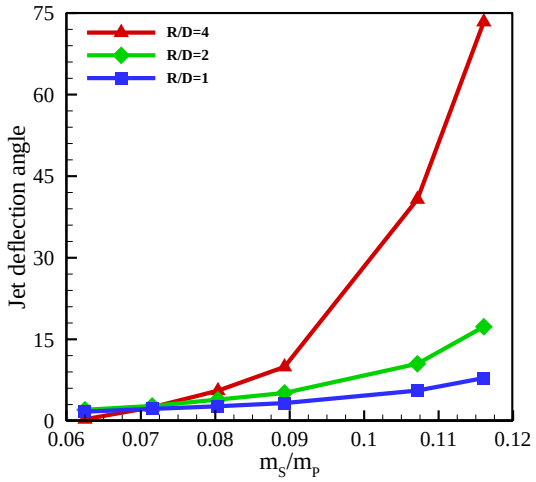

Figure 6: Jet deflection angle at different mass flow and Coanda surface radius ratio at constant h/D=0.125 and g/D=0.0625.

If the pressure is low enough, the jet remains attached to the curved surface. The effects of flow entry and surface friction reduce the flow velocity, which leads to a gradual increase in surface pressure and a decrease in the radial pressure gradient. When there is a flow with high

momentum next to the tangential flow, it causes the tangential flow to be pulled towards itself. By increasing the ratio of mass flow rate to 0.0715, the deviation angle increases for all three tested radiuses. However, depending on the radius of the outlet Coanda surfaces the variation will present different trends. For a radius of R/d=4 the increase of the jet deflection angle due to the growth of the mass flow ratio it is quite more steep and abrupt. As the results indicate, this behavior has a direct relationship with the increase of the Coanda surface radius. Up to the mass flow ratios of 0.09, the variation of the deviation angle with the increase of the mass flow ratio is almost linear. Above this value, for all 3 radius ratios, the deviation angle starts to increase faster following a different evolution trend. For R/d=4, by increasing the mass flow ratio from 0.09 to 0.107, the flow deviation increases about 8 times, following more an exponential trend. However, the value of this nonlinearity depends on two parameters, the ratio of radius to diameter and the value of mass flow ratio.

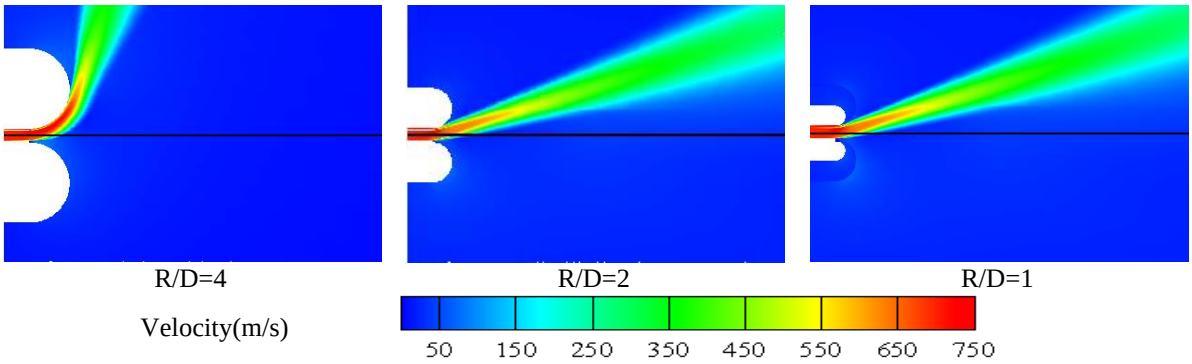

Figure 7: Jet deflection angle at different mass flow and Coanda surface ratio.

3.2.2 Various secondary flow height ratio

Fig. 8 shows the relationship between the angle of the thrust vector for different height between the primary and secondary flows for various mass flow ratios. When the secondary flow is not applied, the plasma jet exits from the plasma torch device without any deviation. However, by applying the secondary flow, the plasma jet tends to attach to the Coanda surface and starts to deflect. The results show that for secondary flow height ratios of 0.125, 0.1875 and 0.25mass, mass flow ratios below 0.0625, 0.08 and 0.09, respectively, will result in negative thrust vector angles. This means that, below the said values, the control method enters in an inactive region where it becomes ineffective and might even deflect the flow in an oppositive direction. In such a case, the secondary flow separates from the Coanda surface earlier and the inverse Coanda effect occurs (negative vector angle). Due to this effect, the primary jet deflects in the opposite direction instead of deflecting in the expected direction. In this case, the primary jet with higher velocity entrains the secondary flow inside, and instead of sticking to the surface of the Coanda, it separates from the surface. The pressure difference area created on the two sides of the main flow causes the main jet velocity distribution to be opposite to the Coanda surface.

By increasing the mass flow ratio, we start operating in the active control region and the Coanda effect starts to be achieved as desired. The flow enters the region where the expected deviation angle can be increased with the growth of the mass flow ratio and, with that,

continuous control of the main jet can be achieved. Moreover, the results demonstrate that by increasing the secondary flow height a larger plasma jet deviation angle can be achieved.

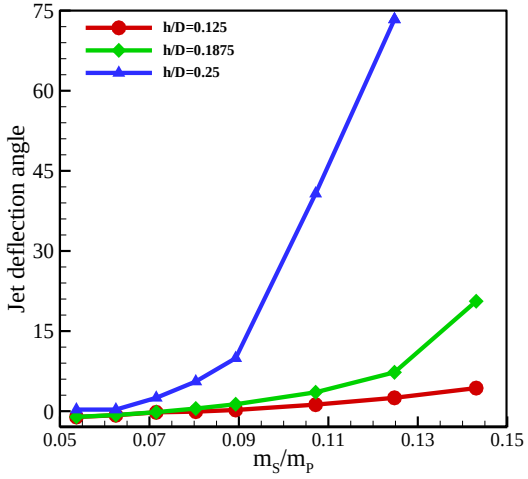

Figure 8: Jet deflection angle at different mass flow and various secondary flow heights.

3.2.3 Various gap between secondary and primary flow ratio

Figure 10 shows the deflection angle variation for different gaps and various mass flow rates between the primary and secondary flows. In Figure 9 the velocity contours are shown for different gaps and a mass flow ratio of 0.117, since from this was the mass flow ratio that demonstrated larger differences between the different gaps tested. Regarding to the gap between the two flows, for mass flow ratios up to 0.09 there is no visible influence on the jet deflection angle, demonstrating very similar values. However, for mass flow ratios above 0.09, the results indicate that lower gaps between the two flows allow to optimize the flow vectorizing effect.

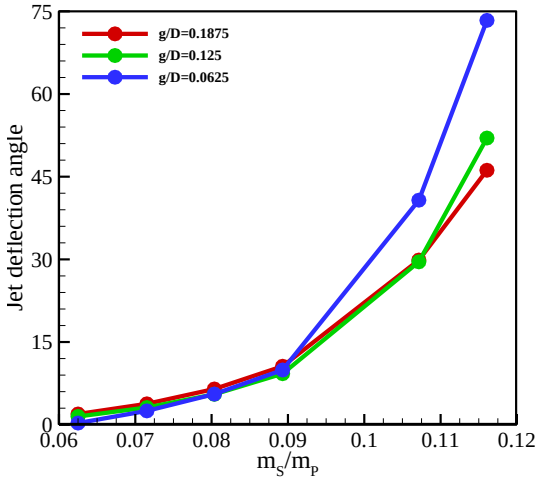

Figure 9: Jet deflection angle at different mass flow ratios and different gaps between secondary and primary flows.

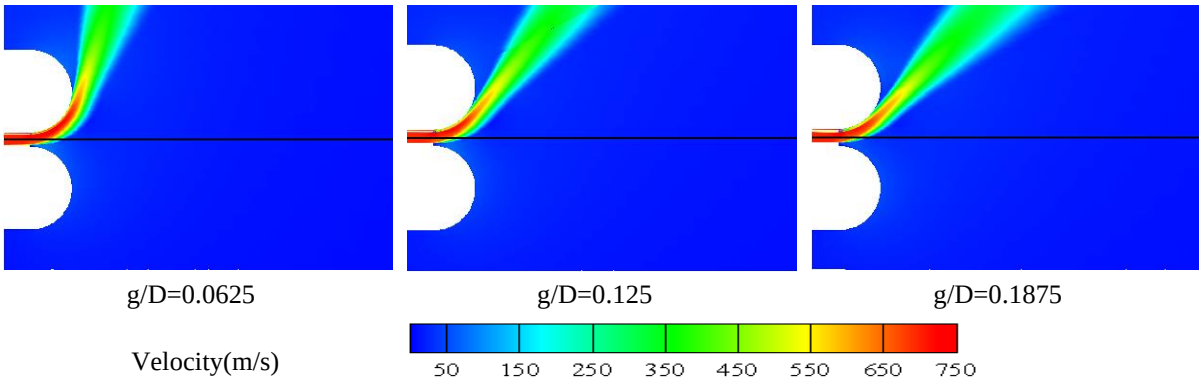

Figure 10: Jet deflection angle at different mass flow and gap between secondary and primary flow.

The main difference observed for different gaps was found for a flow ratio of 0.117 as it is shown in Figure 10 by the velocity distribution contours. As it is shown all the three tested gaps allowed to effectively vectorize and control the plasma jet. However, in the case of lower gap, we observed that the plasma jet at the outlet is better attached to the surface, and thus, the Coanda effect is improved. With this, we conclude that lower gaps between the two flows allow to achieve a better control over the outlet flow vectorization.

4 CONCLUSIONS

In the current work, the fluidic thrust vectoring method was studied for controlling the plasma jet direction at the outlet of a plasma torch device. Therefore, the main purpose of this study is the numerical investigation to deflect plasma torch jets using the Coanda effect. A tridimensional plasma torch simulation was performed in order to obtain the important information about temperature and velocity. The information obtained in the first simulation was then used as boundary condition for the bidimensional simulations of the plasma jet at the outlet of the nozzle. This approached allowed us to perform the analysis with lower computational power. Simulations allowed to study the effect of different important parameters on the jet deflection angle. The obtained results allowed to conclude that the deflection angle of the main flow increases with the increase of the mass flow ratio. This was observed for all the test cases performed independently of the Coanda surface radius, secondary flow height or gap between the flows. Furthermore, the results demonstrated that, at fixed mass flow ratio, the deflection angle of the main flow increases with the increase in the Coanda surface ratio or with the increase of the secondary flow height. In addition, it was observed that for low mass flow ratios the gap between the flows has almost no influence on the deflection angle. However, for flow ratios above 0.09 the gap will affect the vectorization of the outlet flow and we could conclude that lower gaps will allow to achieve larger deflection angles.

ACKNOWLEDGEMENTS

This work was supported by the Project “Smart Sustainable Farms Foods and Trade European Digital Innovation Hub”- SFT-EDIH”. Aditional support was provided by and by C-MAST (Center for Mechanical and Aerospace Science and Technology), Research Unit No. 151, project grant number UIDB/00151/2020 (https://doi.org/10.54499/UIDB/00151/2020) and

grant number UIDP/00151/2020 (https://doi.org/10.54499/UIDP/00151/2020).

REFERENCES

[1] M.S. Francis, Air Vehicle Management with Integrated Thrust-Vector Control, AIAA Journal, 56 (2018) 4741–4751. https://doi.org/10.2514/1.J056768.
[2] M. Abdollahzadeh, F. Rodrigues, J.C. Pascoa, P.J. Oliveira, Numerical design and analysis of a multi-DBD actuator configuration for the experimental testing of ACHEON nozzle model, Aerosp Sci Technol 41 (2015) 259–273. https://doi.org/10.1016/J.AST.2014.12.012.
[3] J.C. Páscoa, A. Dumas, M. Trancossi, P. Stewart, D. Vucinic, A review of thrust-vectoring in support of a V/STOL non-moving mechanical propulsion system, Central European Journal of Engineering 3 (2013) 374–388, https://doi.org/10.2478/S13531-013-0114-9.
[4] S. Afridi, T.A. Khan, S.I.A. Shah, T.A. Shams, K. Mohiuddin, D.J. Kukulka, Techniques of Fluidic Thrust Vectoring in Jet Engine Nozzles: A Review, Energies 2023, Vol. 16, Page 5721 16 (2023) 5721. https://doi.org/10.3390/EN16155721.
[5] C. Lubert, On some recent applications of the Coanda effect to acoustics, Proceedings of Meetings on Acoustics 11 (2011) 40006. https://doi.org/10.1121/1.3694201.
[6] B.G. Newman, The Deflexion of Plane Jets by Adjacent Boundaries - Coanda Effect, in: Boundary Layer Control Principles, Pergamon Press: Oxford, 1961: pp. 232–264.
[7] F. Rodrigues, J.C. Páscoa, F. Dias, M. Abdollahzadeh, Plasma Actuators for Boundary Layer Control of Next Generation Nozzles, ASME International Mechanical Engineering Congress and Exposition, Proceedings (IMECE) 1–2015 (2016). https://doi.org/10.1115/IMECE2015-52193.
[8] P.W. Carpenter, P.N. Green, The aeroacoustics and aerodynamics of high-speed Coanda devices, Part 1: Conventional arrangement of exit nozzle and surface, J Sound Vib 208 (1997) 777–801. https://doi.org/10.1006/JSVI.1997.1202.
[9] R. Neuendorf, I. Wygnanski, On a turbulent wall jet flowing over a circular cylinder, J Fluid Mech 381 (1999) 1–25. https://doi.org/10.1017/S0022112098003668.
[10] A. Gross, H.F. Fasel, Coanda Wall Jet Calculations Using One- and Two-Equation Turbulence Models, AIAA Journal, 44 (2012) 2095–2107. https://doi.org/10.2514/1.3506.
[11] A. Dumitrache, F. Frunzulica, T.C. Ionescu, A. Dumitrache, F. Frunzulica, T.C. Ionescu, Mathematical Modelling and Numerical Investigations on the Coanda Effect, Nonlinearity, Bifurcation and Chaos - Theory and Applications (2012). https://doi.org/10.5772/50403.
[12] J.C. Páscoa, F.F. Rodrigues, S.S. Das, M. Abdollahzadeh, A. Dumas, M. Trancossi, M. Subhash, Exit Flow Vector Control on a Coanda Nozzle Using Dielectric Barrier Discharge Actuator, ASME International Mechanical Engineering Congress and Exposition, Proceedings (IMECE) 1 (2015). https://doi.org/10.1115/IMECE2014-38915.
[13] P. Juvet, Control of high Reynolds number round jets, Stanford University, 1993.
[14] M.S. Mason, W.J. Crowther, Fluidic thrust vectoring for low observable air vehicles, 2nd AIAA Flow Control Conference (2004). https://doi.org/10.2514/6.2004-2210.
[15] A. Banazadeh, F. Saghafi, M. Ghoreyshi, P. Pilidis, Experimental and computational investigation into the use of co-flow fluidic thrust vectoring on a small gas turbine, The Aeronautical Journal 112 (2008) 17–25. https://doi.org/10.1017/S0001924000001950.
[16] A. Al-asady, A. Abdullah, Fluidics Thrust Vectoring Using Co-Flow Method

Nomenclature, Al-Nahrain Journal for Engineering Sciences 20 (2017).
[17] M.S. Mason, W.J. Crowther, Fluidic thrust vectoring for low observable air vehicles, 2nd AIAA Flow Control Conference (2004). https://doi.org/10.2514/6.2004-2210.
[18] S.M. Ahmad, S.M. Siddique, M.S. Yousaf, M. Tariq, M.I. Khan, M.A. Alam, Computational and experimental investigation of fluidic thrust vectoring actuator, Journal of the Brazilian Society of Mechanical Sciences and Engineering 40 (2018) 1–11. https://doi.org/10.1007/S40430-018-1248-8.
[19] E. Gomez, D.A. Rani, C.R. Cheeseman, D. Deegan, M. Wise, A.R. Boccaccini, Thermal plasma technology for the treatment of wastes: A critical review, J Hazard Mater 161 (2009) 614–626. https://doi.org/10.1016/J.JHAZMAT.2008.04.017.
[20] M. Ito, J.S. Oh, T. Ohta, M. Shiratani, M. Hori, Current status and future prospects of agricultural applications using atmospheric-pressure plasma technologies, Plasma Processes and Polymers 15 (2018) 1700073. https://doi.org/10.1002/PPAP.201700073.
[21] K.O.; Shvydyuk, J.; Nunes-Pereira, F.F.; Rodrigues, A.P. Silva, K.O. Shvydyuk, J. Nunes-Pereira, F.F. Rodrigues, A.P. Silva, Review of Ceramic Composites in Aeronautics and Aerospace: A Multifunctional Approach for TPS, TBC and DBD Applications, Ceramics 2023, Vol. 6, Pages 195-230 6 (2023) 195–230. https://doi.org/10.3390/CERAMICS6010012.
[22] F. Rodrigues, M. Abdollahzadehsangroudi, J. Nunes-Pereira, J. Páscoa, Recent Developments on Dielectric Barrier Discharge (DBD) Plasma Actuators for Icing Mitigation, Actuators 2023, Vol. 12, Page 5 12 (2022) 5. https://doi.org/10.3390/ACT12010005.
[23] A. D'Angola, G. Colonna, E. Kustova, Editorial: Thermal and Non-Thermal Plasmas at Atmospheric Pressure, Front Phys 10 (2022) 852905. https://doi.org/10.3389/FPHY.2022.852905.
[24] J. Nunes-Pereira, F.F. Rodrigues, M. Abdollahzadehsangroudi, J.C. Páscoa, S. Lanceros-Mendez, Improved performance of polyimide Cirlex-based dielectric barrier discharge plasma actuators for flow control, Polym Adv Technol 33 (2022) 1278–1290. https://doi.org/10.1002/PAT.5600.
[25] K.O. Shvydyuk, F.F. Rodrigues, J. Nunes-Pereira, J.C. Páscoa, S. Lanceros-Mendez, A.P. Silva, Long-lasting ceramic composites for surface dielectric barrier discharge plasma actuators, J Eur Ceram Soc 43 (2023) 6112–6121. https://doi.org/10.1016/J.JEURCERAMSOC.2023.05.040.
[26] B. Haertel, T. von Woedtke, K.D. Weltmann, U. Lindequist, Non-Thermal Atmospheric-Pressure Plasma Possible Application in Wound Healing, Biomol Ther (Seoul) 22 (2014) 477. https://doi.org/10.4062/BIOMOLTHER.2014.105.
[27] M. Moreau, N. Orange, M.G.J. Feuilloley, Non-thermal plasma technologies: New tools for bio-decontamination, Biotechnol Adv 26 (2008) 610–617. https://doi.org/10.1016/J.BIOTECHADV.2008.08.001.
[28] M. Moreira, F. Rodrigues, S. Cândido, G. Santos, J. Páscoa, Development of a Background-Oriented Schlieren (BOS) System for Thermal Characterization of Flow Induced by Plasma Actuators, Energies 2023, Vol. 16, Page 540 16 (2023) 540. https://doi.org/10.3390/EN16010540.
[29] N. Venkatramani, Industrial plasma torches and applications on JSTOR, Curr Sci 83 (2002) 254–262. https://www.jstor.org/stable/24106883 (accessed August 6, 2024).

[30] J.M. Sankovic, D.T. Jacobson, Performance of a miniaturized arcjet, 31st Joint Propulsion Conference and Exhibit (1995). https://doi.org/10.2514/6.1995-2822.
[31] B. Wollenhaupt, Q.H. Le, G. Herdrich, Overview of thermal arcjet thruster development, Aircraft Engineering and Aerospace Technology 90 (2018) 280–301. https://doi.org/10.1108/AEAT-08-2016-0124.
[32] A.B. Murphy, C.J. Arundelli, Transport coefficients of argon, nitrogen, oxygen, argon-nitrogen, and argon-oxygen plasmas, Plasma Chemistry and Plasma Processing 14 (1994) 451–490. https://doi.org/10.1007/BF01570207.
[33] V. Colombo, E. Ghedini, P. Sanibondi, Thermodynamic and transport properties in non-equilibrium argon, oxygen and nitrogen thermal plasmas, Progress in Nuclear Energy 50 (2008) 921–933. https://doi.org/10.1016/J.PNUCENE.2008.06.002.
[34] R. Huang, H. Fukanuma, Y. Uesugi, Y. Tanaka, An improved local thermal equilibrium model of DC Arc plasma torch, IEEE Transactions on Plasma Science 39 (2011) 1974–1982. https://doi.org/10.1109/TPS.2011.2163828.